Carbon Xerogel and Manganese Oxide Capacitive Materials for Advanced Supercapacitors

F. Lufrano[1,], P. Staiti[1], E.G. Calvo[2], E.J. Juárez-Pérez[2], J.A Menéndez[2], A. Arenillas[2]*

[1] CNR-ITAE, Istituto di Tecnologie Avanzate per L'Energia "Nicola Giordano", Via Salita S. Lucia, 5 – 98126 Messina, Italy
[2] Instituto Nacional del Carbón, CSIC, Apartado 73, E-33080, Oviedo, Spain
[*]E-mail: Lufrano@itae.cnr.it

Symmetric supercapacitors (SSC) and asymmetric supercapacitors (ASC) that use carbon xerogels with different porous textures as negative electrode and manganese oxide as positive electrode were investigated. The electrochemical performance of symmetric supercapacitors with carbon xerogel electrodes was mainly influenced by the textural characteristics of the carbon, pore size distribution being the property that has the strongest influence on the capacitance performance. The asymmetric supercapacitor showed an excellent capacitance performance (i.e. 213 F g^{-1}) when a chemical activated carbon xerogel with a high S_{BET} (i.e. 2360 m^2 g^{-1}) was used as negative electrode and high performing oxide-based manganese as positive electrode, thereby demonstrating that carbon xerogels and manganese oxide have potential applications in supercapacitor devices.

1. INTRODUCTION

Supercapacitors are energy storage devices, which have intermediate characteristics between batteries and traditional capacitors [1-3]. Unlike batteries, the charge/discharge mechanism of electrochemical supercapacitors is mainly of a capacitive type. These devices can be built according to two different configurations: (i) symmetric (SSC), where the two electrodes (positive and negative) are identical, and (ii) asymmetric (ASC), where the two electrodes are different in terms of materials, loading and/or composition. In these supercapacitors two main capacitive storage processes can take place, one based on the formation of a double layer of charges that arises at the interface of the electrode and the electrolyte solution and the other originated from the charge-transfer process in the

active component of the electrode through a reversible redox reaction (faradaic). This reaction causes a change in the state of oxidation of the material (pseudocapacitive process). The use of materials with pseudocapacitive properties in one electrode coupled with materials with purely capacitive properties in the other electrode increases the energy density of the supercapacitor and enlarges the working voltage window up to 2 V in aqueous electrolytes [4-5]. Manganese oxide, a material well known for its pseudocapacitive properties, has attracted growing interest in recent years as a possible alternative to the more costly ruthenium oxide for use in asymmetric (or hybrid) supercapacitors.

Carbon-based active materials with a high surface area are nowadays commonly used in the electrodes of supercapacitors and for this reason they are also known as electric double layer capacitors (EDLCs). These materials are highly competitive due to their relatively low cost and their good electronic conductivity (c.a. 0.1–1 S cm^{-1}), a property that endows the capacitors with a low internal resistance.

Carbon gels are porous materials that are highly sensitive to the conditions in which they are synthesized. They are very easy to tailor in terms of shape, porous texture and surface chemistry [6]. These features, along with their extremely low inorganic matter content, make them more suitable for use in supercapacitors than traditional activated carbons. Moreover, they have a low mass density and a high electrical conductivity which also make them ideally appropriate for use in supercapacitors [6]. Carbon gels can be obtained by different procedures [6], but the preparation basically consists of three steps: (i) gel synthesis, involving the formation of a three-dimensional polymer in a solvent (gelation), followed by a curing period, (ii) gel drying, where the solvent is removed to obtain an organic gel, and finally (iii) pyrolysis under an inert atmosphere to form the porous carbon material, i.e. the so-called carbon gel. Resorcinol-formaldehyde (RF) aqueous gels are among the most studied systems [6]. Most of the published works on RF gels agree that the synthesis and drying processes are the steps that define the size and volume of the mesopores and macropores in the final carbon gels and that the development of the micropores takes place during the subsequent pyrolysis step [7]. The meso- or macroporosity formed during the synthesis is barely altered during thermal stabilization (i.e. the pyrolysis step). The microporosity created during the pyrolysis can be increased through an activation process. These carbon materials are composed of interconnected sphere-like nodules, whose size can be regulated by the synthesis conditions. Consequently, the size of the voids between the nodules can be tailored [7-8]. The micropores are formed within the nodules by removing some of the labile matter during pyrolysis. RF carbon gels usually have surfaces of around 600-700 m^2 g^{-1}, whereas activated carbon surfaces can exceed 2000 m^2 g^{-1}. However, to overcome this limitation, carbon gels can be chemically activated for specific applications where high surface areas are required.

In this work, carbon xerogels with different meso/macropore textures were prepared by varying the initial pH of the resorcinol-formaldehyde aqueous solution. The organic gels were first dried by evaporation of the solvent and then pyrolysed. In order to develop the microporosity and increase the surface area of the final carbonaceous materials, chemical activation with phosphoric acid was performed. The effect of the textural properties of the gels on their performance in the electrodes of supercapacitors was evaluated by electrochemical tests. Although carbon gels have already been studied as active material in double layer capacitors [9-12] and are employed in commercially available supercapacitors, to the best of our knowledge they have not never been used in

asymmetric/hybrid supercapacitors. Here, we report the synthesis of carbon xerogel materials and the development of electrodes for supercapacitors with two possible configurations: a) symmetric (SSC) - where two electrodes of carbon xerogel material were used, and b) asymmetric (ASC) – where carbon xerogel was used as active material in a negative electrode coupled to a manganese oxide-based positive electrode.

2. EXPERIMENTAL

2.1. Preparation of carbon xerogels

Aqueous organic gels were synthesised by the polycondensation of resorcinol (R) with formaldehyde (F) in water (W). Sodium hydroxide (C) was used as basification agent. The resorcinol (99%) by VWR International Eurolab S.L. (Barcelona, Spain), was first dissolved in deionised water in a sealed flask under magnetic stirring. Formaldehyde (solvent: 37% wt. water and 10-15% wt. methanol) was added to the mixture under magnetic stirring and kept under stirring until a homogeneous solution was obtained.

All the gels were synthesised using an R/F molar ratio equal to the stoichiometric value (0.5) and a fixed dilution ratio, D (i.e. the total solvent/reactant molar ratio) of 5.7. It should be noted that the "total solvent" includes the deionised water from the initial solution, and the water and methanol contained in the formaldehyde solution, whilst "reactant" refers to the resorcinol and formaldehyde. Methanol is a stabilizer that prevents the formaldehyde molecules from undergoing polymerisation during storage. Three different organic gels were synthesised under different initial solution pHs (i.e. 5.8, 6.3 and 6.5). In the text these carbon samples are named as CX5.8, CX 6.3 and CX6.5, respectively. The solutions were placed in an oven at 85 ℃ for 72 h to undergo gelation and ageing. The aqueous gels obtained were then dried by evaporation, without any pre-treatment, in the same oven at 150 ℃ for 24 h. After drying, the gels were pyrolysed at 800 ℃ under nitrogen flow in a tubular oven, using the following heating program: (i) ramp at 1.7 ℃ min^{-1} to 150 ℃ and hold for 15 min; (ii) ramp at 5 ℃ min^{-1}to 400 ℃ and hold for 60 min; (iii) ramp at 5 ℃ min^{-1} to 800 ℃ and hold for 120 min; and (iv) cool slowly to room temperature.

A carbon xerogel was chemically activated with 75 wt% orthophosphoric acid (from VWR International), using an activating agent/carbon gel mass ratio of 3:1. The mixture was stirred at 85 ℃ for 2 h, and then filtered and dried overnight in an oven at 110 ℃. Next the samples were heated under N$_2$ flow (85 ml min^{-1}) at 5 ℃ min^{-1} up to 450 ℃ and held at this temperature for 2h. Finally the carbon sample were washed with water until pH 6 and dried overnight at 110℃. This final sample was denoted as AOX6.5C.

2.2. Characterization of the carbon xerogels

In order to characterize the porous texture of the samples, carbon dioxide adsorption-desorption isotherms at 0 ℃ and nitrogen adsorption-desorption isotherms at -196 ℃ were performed on a TriStar

3000 Surface Area and Pore Size Analyzer by Micromeritics (Norcross, GA USA). The use of carbon dioxide adsorption at 0 ℃ for the textural characterisation of narrow micropores has already been established as an effective procedure [13] because carbon dioxide adsorption occurs in pores smaller than 0.7 nm, whereas nitrogen cannot enter in pores of such a small size.

The resulting combination of nitrogen and carbon dioxide adsorption isotherms data provide complementary and relevant information about the full micropore range. The Dubinin-Radushkevich (DR) method [14] was applied to the carbon dioxide and nitrogen adsorption isotherms in order to obtain the narrow micropore volume, $V_{DUB-CO2}$, and the wider micropore volume, V_{DUB-N2}, respectively. The BET surface area was also evaluated from the nitrogen adsorption isotherms. The accessible average micropore width, L_0 (nm), was calculated from the expression L_0 (nm) = V_{DUB-N2} ($cm^3 g^{-1}$) 2000/S_{mic} ($m^2 g^{-1}$) [15-16].

However, in the case of the meso-macroporous samples, nitrogen and carbon dioxide adsorption was not used to evaluate the real total pore volume. In this case a mercury porosimeter was employed to determine the pore volume (V_{Hg}) and the mean pore size. The measurements were performed using a Carlo Erba Porosimeter 2000 (Milan, Italy) (after outgassing at 10^{-3} Pa for 2 h. Hg measurements were limited to pores larger than 5.5 nm. The total pore volume, V_T, was considered to be equal to the sum of V_{Hg} and V_{DUB-N2}.

2.3. Preparation of electrodes for symmetric and asymmetric supercapacitors

Both the carbon xerogel and the manganese oxide electrodes were prepared by a casting method. The carbon xerogel based electrodes were prepared by spreading over a glass plate a slurry containing the carbon gel, graphite fibres, poly vinylidene fluoride (PVDF) binder and the N,N-dimethylacetamide (DMA) solvent.

The manganese oxide based electrode was prepared by applying a slurry composed of manganese oxide, carbon black, graphite fibres, PVDF binder and DMA. Both of these self-supporting electrodes were dried at 70°C and then thermally treated at 160 °C for 20 min to improve their mechanical strength. The PVDF (poly vinylidene fluoride) binder (Aldrich) was used as a solution of 2 wt% in DMA. The carbon black (Shawinigan Acetylene Black by Chevron Phillips) with a purity >99.9 % and a surface area of 75 $m^2 g^{-1}$ was employed as conductive additive material in the MnO_2 electrodes. The graphite fibres were obtained by milling a carbon fabric Avcarb 1071 HCB furnished by Ballard Material Products, Inc. (MA, USA) in a high speed grinder.

The amount of carbon and manganese oxide loaded into the electrodes was similar to that used in real supercapacitors. Thus, 3.6 mg cm^{-2} of MnO_2 was loaded into the positive electrodes whereas 8 ± 2 mg cm^{-2} of carbon gel was loaded into the negative electrodes. The composition of the materials in the electrodes was: 70% MnO_2 – 10% acetylene black – 10% graphite fibres – 10% PVDF, for the positive electrode; 80% carbon gel– 10% graphite fibres – 10% PVDF for the negative electrode [17]. A ready-to-operate 4 cm^2 supercapacitor was prepared by coupling the two electrodes to a porous polymeric film separator (thickness: 50 μm x 2 separators) impregnated with 0.1 M Na_2SO_4.

2.4. Electrochemical characterisation of the symmetric and asymmetric supercapacitors

Electrochemical characterization of electrodes in SSC and ASC was carried out in a two-electrode cell connected to a potentiostat/galvanostat Autolab PGSTAT 30 (Eco Chemie BV, The Netherlands). Cyclic voltammetry (CV) tests and galvanostatic charge/discharge (GCD) measurements were performed at different voltage sweep rates and current densities, respectively by cycling in a voltage window from 0 to +1 V for the SSC and between 0 and +1.6 V for the ASC. The electrolyte used in both supercapacitors was 0.1M Na_2SO_4. The electrochemical impedance spectroscopy (EIS) measurements were performed using a Potentiostat PGSTAT 30 fitted with a FRA2 module at frequencies between 10 MHz and 1 mHz and at open circuit voltage (OCV).

3. RESULTS AND DISCUSSION

3.1. Surface and textural properties of the carbon xerogels

The adsorption-desorption isotherms of all the carbon xerogels studied are presented in Figure 1. They show capillary condensation and a hysteresis loop at high relative pressures (p/p°), indicating the presence of mesoporosity [8,18-19]. Furthermore, at low relative pressures the isotherms of the carbon gels CX5.8, CX6.3 and CX6.5 are very similar, which indicates that the differences between these samples are due mainly to the mesoporosity and not to the microporosity. The BET specific surface area, pore volume, and other micro-textural parameters of the carbons determined by nitrogen adsorption-desorption are summarized in Table 1.

Table 1. Textural properties of the carbon xerogels studied

Sample	pH	S_{BET} $(m^2 g^{-1})$	S_{mic} $(m^2 g^{-1})$	V_{DUB-N2} $(cm^3 g^{-1})$	$V_{DUB-CO2}$ $(cm^3 g^{-1})$	L_0[a] (nm)	V_{Hg}[b] $(cm^3 g^{-1})$	V_T[c] $(cm^3 g^{-1})$
CX5.8	5.8	670	500	0.26	0.25	1.04	1.44	1.72
CX6.3	6.3	661	464	0.26	0.24	1.12	0.90	1.16
CX6.5	6.5	651	409	0.26	0.22	1.27	0.57	0.83
AOX6.5C	6.5	2360	706	0.76	0.34	2.1	-	1.56[d]

[a] Calculated from the expression L_0 (nm) = V_{DUB-N2} $(cm^3 g^{-1})$ 2000/S_{mic} $(m^2 g^{-1})$
[b] Pore volume determined by mercury porosimetry of pores between 5.5 and 100 nm
[c] Total pore volume (V_T) calculated by the sum of V_{Hg} and V_{DUB-N2}
[d] In this case the total pore volume is the volume at the saturation point (p/p⁰) in the N_2 adsorption isotherm
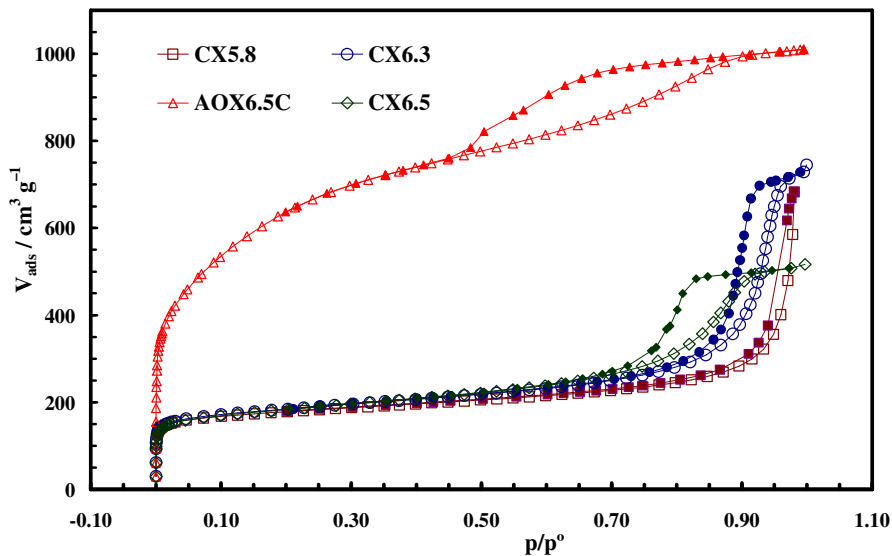
Figure 1. Nitrogen adsorption (open symbol)/desorption (filled symbol) isotherms for synthesized carbon xerogels
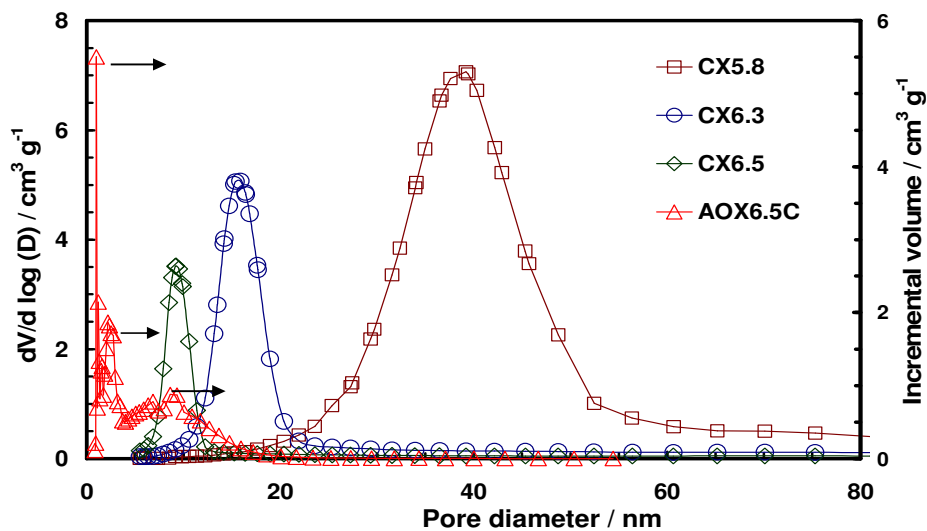

Figure 2. Pore size distributions of the different carbon xerogels.

It can be seen that the S_{BET}, S_{mic} and $V_{DUB-CO2}$ decrease slightly as the pH of the initial solution increases. The accessible average micropore width (L_0) also increases slightly with the pH. This indicates that the used synthesis conditions slightly modify the microporosity and the surface area of the carbon xerogels. The pH of the initial solution mainly affects the meso/macroporosity, as can be inferred from the high relative pressure zones of the N_2 adsorption isotherms and from the mercury porosimetry characterization.

Further differences in the porous texture of the carbon xerogels can be obtained from the mercury porosimetry results. Figure 2 shows the pore size distribution of the carbon xerogels as determined by mercury porosimetry. Although the synthesized xerogels have similar BET surface areas and micropore volumes, their meso/macropore size distribution is clearly correlated to the pH of the initial solutions. Therefore, as the pH increases, their meso/macropore textures start to differ. The average pore diameter decreases as the pH of the precursor solution increases (i.e., 38, 16 and 9 nm for CX5.8, CX6.3 and CX6.5, respectively) and the total pore volume, V_T, as estimated by mercury porosimetry and the DR method ($V_T = V_{Hg} + V_{DUB-N2}$) also follows the same decreasing trend (i.e., 1.72, 1.16 and 0.83 cm^3 g^{-1} for CX5.8, CX6.3 and CX6.5, respectively).

Also the chemical activated carbon xerogel AOX6.5C shows high N_2 adsorption capacity at low p/p^0 indicating that this carbon is highly microporous, although the hysteresis loop at high p/p^0 also indicates the presence of mesoporosity. The sample AOX6.5C has a multimodal pore size distribution, as can be seen from Figure 2. Values of mesopores size was found to be at 10 nm and at 2.3 nm indicating that after chemical activation in phosphoric acid the AOX6.5C has preserved the mesoporous features, but increased considerably its microporosity ($V_{mi}DR = 0.76$ cm^{3}g^{-1}). The AOX6.5C sample has also a high V_T (1.56 cm^{3}g^{-1}) and S_{BET} of 2360 cm^{2}g^{-1} (see Table 1).

3.2. Cyclic voltammetry studies of carbon xerogels in symmetric supercapacitors

Figure 3 shows the curves of specific capacitance (C_s) as a function of the cell voltage for the carbon xerogel based supercapacitors.
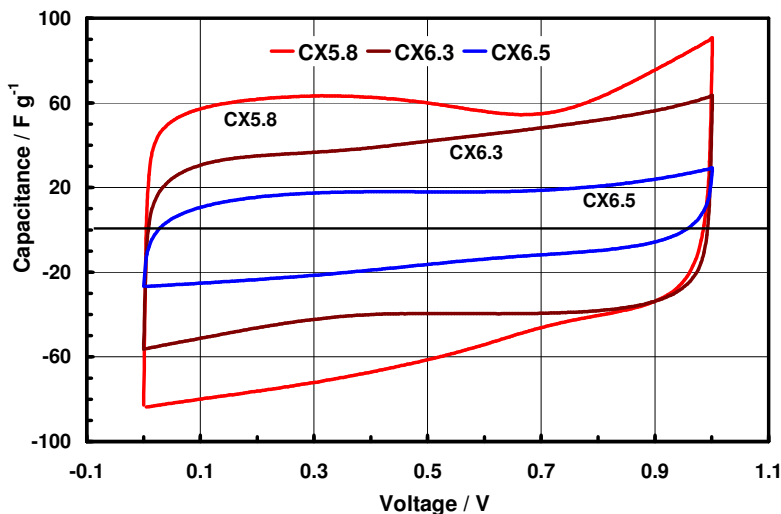

Figure 3. Capacitance curves versus potential for carbon xerogel-based supercapacitors. Voltage sweep rate:10 mVs^{-1}.

These curves show that the CX5.8 based supercapacitor exhibits a higher specific capacitance than the other two carbons. However, the supercapacitors loaded with CX6.3 and CX6.5 produce

voltammograms with more rectangular shapes. In the case of xerogel CX5.8 there is a deviation from pure capacitive behavior with the appearance of a broad peak of uncertain origin in the 0 to 0.4 V range. The presence of this broad peak could be due to parallel redox reactions providing additional pseoudocapacitance to the double layer capacitance, since it is known that surface functional groups present on the surface of carbons can supply strong pseudocapacitance by means of faradaic processes [20]. Whereas the pseudocapacitance derived from oxygenated species is important in acid (H_2SO_4) and basic (KOH) electrolytes, it is absent or very low in neutral aqueous electrolyte [21-22]. It is also well known that the surface chemistry of non graphitic carbons, such as carbon xerogels, can have a strong influence on electronic resistance and consequently on electrochemical performance. The capacitance results obtained for these capacitors show that they bear an evident correlation to the pore size of the xerogels, which in turn depends on the pH of the initial synthesis solution. Higher specific capacitance values were obtained from carbon xerogel CX5.8 (71 F g^{-1}), compared to those of CX6.3 (50 F g^{-1}) and CX6.5 (about 30 F g^{-1}). These values were unexpectedly low in consideration that the surface-texture properties indicated practically the same specific surface area for all the samples (650-670 m^2 g^{-1}). These low values of capacitance are clearly due to the relatively low specific surface area of the carbon samples employed. However, the aim of this work was not to find a breakthrough carbon material but to evaluate the influence of the pore size distribution (PSD) of carbons of similar specific surface area (S_{BET}).

3.3. Electrochemical impedance spectroscopy (EIS) study of carbon xerogels

EIS is an important analytical technique that can be used to establish the characteristic frequency response of supercapacitors from the speed at which the ionic and electronic charges are moving inside the pores of carbon electrodes under one single-sine or multi-sine signal of alternate current (AC).
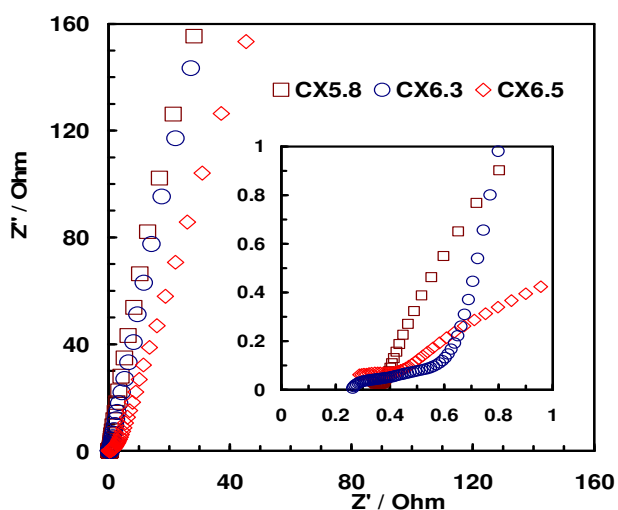

Figure 4. Nyquist plot of the different carbon xerogels. The inset shows the high-frequency region of impedance.

The Nyquist impedance plots corresponding to the different carbon xerogel-based supercapacitors are shown in Figure 4. At low frequencies (mHz range, upper region of large graph), the points depict shapes near to those of ideal capacitors. The inset in the figure shows the impedance behaviour of all the supercapacitors at high frequencies. The impedance plots in the inset have slight loops of different amplitude at high frequency that could be due to the charge transfer process and/or to the different contact resistances [1]. At high frequencies, the resistance characteristics of the supercapacitors are expressed as the so-called electric series resistance (ESR), a term which includes electrolyte resistance, collector/electrode contact resistance and the resistance of the electrode/electrolyte interface. The capacitors loaded with carbon xerogel CX5.8 show lower impedance compared to those loaded with CX6.3 and CX6.5, in agreement with the capacitance results presented in Figure 3.
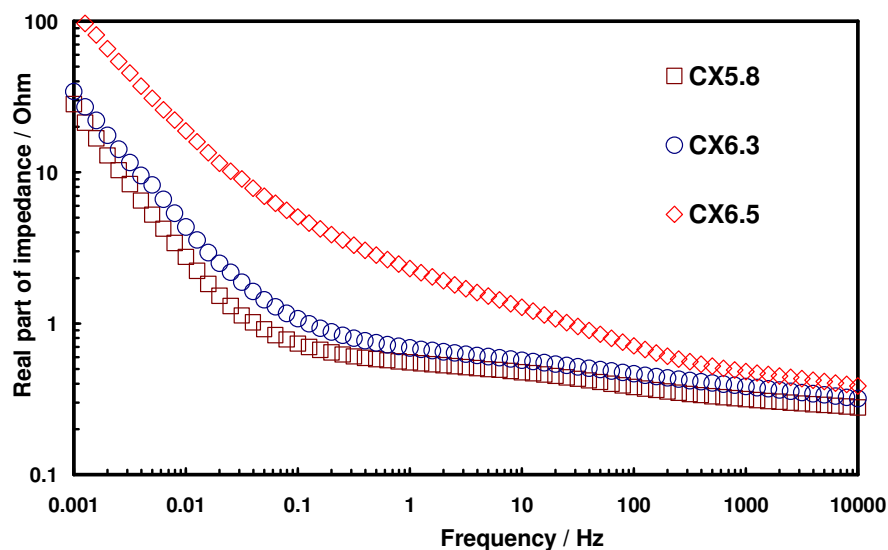

Figure 5. Real part of impedance as a function of frequency for the different carbon xerogel-based supercapacitors.

The differences in impedance behavior are further illustrated in Figure 5, where the real part of impedance, Z', is plotted as a function of frequency. In the high frequency region, kHz, the impedance comes from the resistance of the ionic electrolyte, to which must be added that of the two electrodes and the interface resistance between the electrodes and current collectors.

However, as the frequency decreases other types of resistance appear which cause an increase in the overall supercapacitor resistance. These additional resistances are caused by the penetration of electric signals and the movement of ion species inside carbon pores of different diameter [23-24]. The results in Figure 5 also show that the resistance of sample CX6.5 is very different to that of CX5.8 and CX6.3. The differences between CX5.8 and CX6.3 are also significant. If the resistance behaviour of the xerogels is compared with the potentiometric curves of Figure 3 and the pore-size distribution of

Figure 2 , it can be seen that the highest capacitance is correlated with the lowest resistance and the largest mesopore diameter. The relationship between the capacitance and frequency for the different carbon xerogel electrodes as obtained from the impedance analysis is shown in Figure 6. Table 2 summarizes the characteristics of the electrodes, such as composition, capacitance and ionic resistance. It is surprising to observe such huge differences for carbon xerogel-based supercapacitors even though they were synthesized at different pHs. This is a further confirmation that even if the carbons have a similar BET surface area and microporosity, it is the meso/macropore size distribution that determines the capacitive performance.

Table 2. List of investigated carbon xerogels electrodes with compositions, capacitances and ionic resistances.

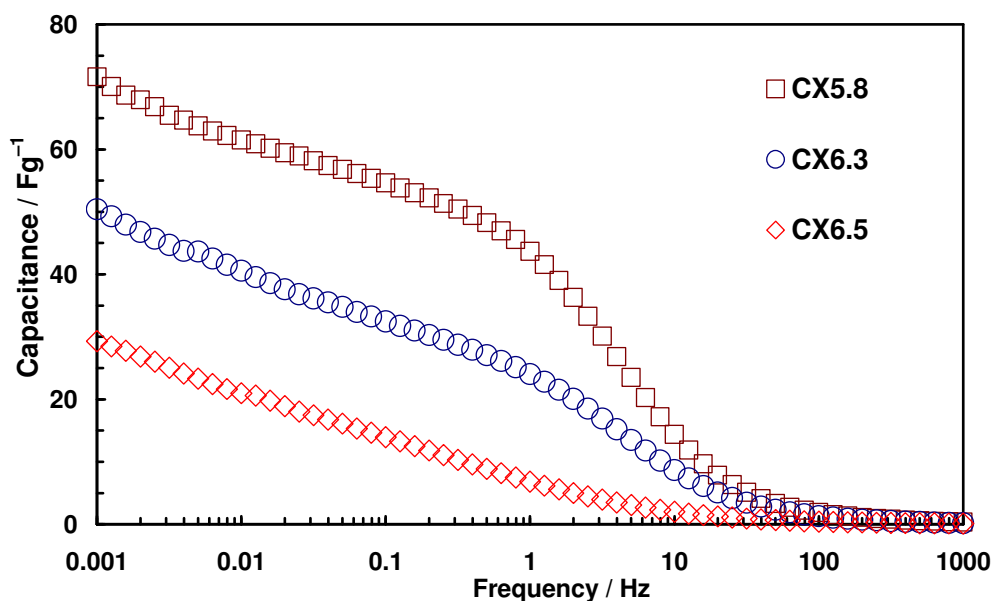| Electrode	Xerogel (%)	Carbon loading mg cm^{-2}	Graphite fibres (%)	PVDF (%)	Specific capacitance CV F g^{-1} 10 mV s^{-1}	Specific capacitance, F g^{-1} at 1 mHz	Ionic Resistance Ohm cm^2
CX5.8	80	7.15	10	10	60	71	1.00
CX6.3	80	8.94	10	10	41	50	1.05
CX6.5	80	6.55	10	10	16	29	1.16

Figure 6. Specific capacitance versus frequency for carbon xerogel based supercapacitors.

Moreover, the impedance analysis of the carbon xerogel-based supercapacitors showed that this analytical technique (EIS) is a quick method for obtaining a great deal of information not only about the electrochemical aspects but also about the textural characteristics of carbons. EIS has already been proposed as a good technique for determining the pore size distributions of carbon materials [25-26].

3.4. Study of chemical activated carbon xerogels in symmetric and asymmetric supercapacitors

Figure 7 shows characteristic voltammograms for SSC and ASC at sweep rates of 5 and 10 mV s^{-1}. The compositions of the electrodes, the capacitance values per electrode and the resistances of the SSC and ASC are presented in Table 3.
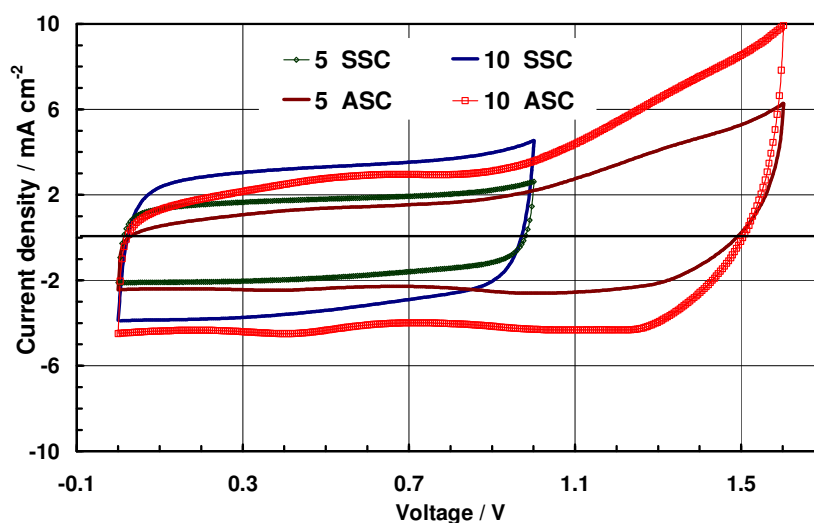

Figure 7. Comparison of the voltammograms of carbon xerogels–based supercapacitors in symmetric (SSC) and asymmetric (ASC) configurations. Voltage sweep rates: 5 and 10 mVs^{-1}. Cell voltage window from 0 to 1 V for SSC and from 0 to 1.6 V for ASC.

The voltammetric behaviour of the symmetric capacitor, AOX6.5C/AOX6.5C, displays almost perfect rectangular shapes, whereas in the voltammograms of ASC, AOX6.5C/MnO$_2$, there is a deviation from this box-like shape due to the pseudocapacitive behavior of the positive electrode, which provides a higher current at high cell voltages. This behaviour of the positive electrode causes the negative electrode to move towards a more negative potential, where an irreversible reduction process is likely to occur. To prevent the high negative polarization and irreversible faradaic processes an appropriate balance between the positive and negative electrode must be obtained. This is because excessive polarization would lead to the evolution and adsorption of hydrogen in the negative electrode as well as to the evolution of oxygen and excessive oxidation of the manganese oxide toward undesired oxide species in the positive electrode [4-5, 27-29]. A comparison between the two different configurations shows that, at the same sweep rate, ASC is delivering a higher capacitance than the SSC

because of the pseudocapacitance originating from the redox process in the positive electrode. Additional advantages provided by the ASC are a higher energy density, since the increase in energy is proportional to the square of the voltage ($E=1/2\ CV^2$). Yet another advantage is the higher volumetric power (kW cm^{-3}) and energy density (Wh cm^{-3}) resulting from the reduced thickness of the positive electrodes, i.e., approximately 140 µm vs 280 µm for the negative electrode. The difference in thickness is due to the higher density and lower load of MnO_2 material (3.6 mg cm^{-2}) compared to that of the carbon negative electrode (≈ 9.6 mg cm^{-2}).

Table 3. Electrochemical characteristics of the carbon xerogel electrodes in symmetric and asymmetric configuration of supercapacitors

Electrodes	Carbon xerogel (%)	Carbon (MnO_2) loading (mg m^{-2})	Thickness Electrode µm	Graphite Fibres (%)	PVDF (%)	Average capacitance by CV[a] (F g^{-1})	Average capacitance by G-CD[a] (F g^{-1})	Ionic Resistance (Ohm cm^2)
AOX6.5C		7.7 (-)	250					
	80			10	10	86	90	2.40
AOX6.5C		8.5 (+)	270					
AOX6.5C		9.56 (-)	280					118
	80			10	10	162	213	0.28
MnO2		3.62 (+)	140					290

[a]The capacitance is that for one electrode and is obtained as weighted average between the weights of the negative and positive electrode active material.
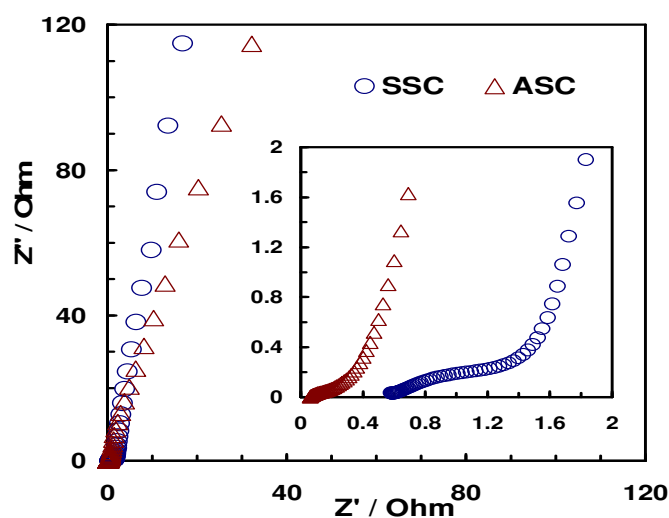

Figure 8. Nyquist plots for the SSC and the ASC in two electrode systems. The inset shows the high frequency region of impedance.

Figure 8 shows the Nyquist plots for the SSC and ASC with an open circuit voltage (OCV). At high frequencies the two plots show small semicircles of different amplitude (inset) and an almost vertical line at lower frequencies (large graph), indicating capacitive behaviour even though the capacitance of the positive electrode is of a faradaic type. Although the impedance plots do not show whether the capacitance in this ASC is capacitive or faradaic, they show that the impedance of ASC is lower than that of SSC, due to the thinner positive electrode in the ASC.
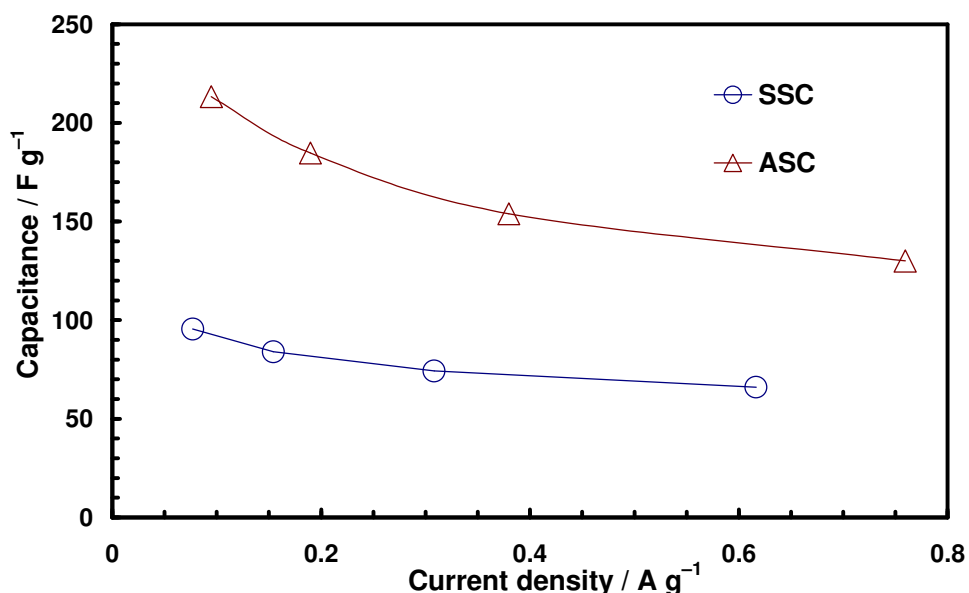

Figure 9. Capacitance behaviour as a function of current density (from G-CD) for the symmetric (SSC) and asymmetric (ASC) supercapacitors.

Figure 9 shows capacitive behaviour as a function of current density in the current range from 0.1 to approximately 0.8 A g^{-1}. These capacitance values were obtained from galvanostatic charge discharge measurements (G-CD) and by calculating the average of the weights of the negative and the positive electrodes (see Table 3), which is considered to be the best way of assessing the specific capacitance (F g^{-1}) of the electrodes of ASCs [30].

The capacitance values (Figure 9) of the ASC are higher than those of the SSC over the entire range of current densities studied. The capacitances of both supercapacitors decrease as the current density increases from 0.1 to 0.8 A g^{-1}. This decrease is about 40% for the ASC, i.e. from 213 to 130 F g^{-1}, whereas that for the SSC is 31%, i.e. from 96 to 66 F g^{-1} for currents varying from 0.08 to 0.6 A g^{-1}. The ASC exhibits a specific energy as high as 15.1 Wh kg^{-1}, whereas that of SSC is only 3.2 Wh kg^{-1} because of its low window cell voltage (1 V vs 1.6 V). Moreover, it is clear that because the capacitance of the ASC is derived from pseudocapacitance (MnO_2 based positive electrode) it is more dependent on the current density than the SSC capacitor, which has two identical capacitive-type electrodes, so that the charge-discharge processes in the SSC should occur at higher rates.

Table 4. Comparison of carbon/MnO$_2$ asymmetric supercapacitors from literature data.

	Negative electrode	Positive electrode	Electrolyte	Max cell voltage, (V)	X = mass$^-$/ mass$^+$ (mg cm^{-2})	Specific capacitance (F g^{-1})	Cycling tests (cycles)	Ionic Resistance Ohm cm^2	Ref.
1	Carbon Xerogel 2500 m^{2}g^{-1}	MnO$_2$	0.1 M Na$_2$SO$_4$	1.6	2.65	213 (+300; -118)	n.d.	0.28	This work
3	AC Maxsorb 2500 m^{2}g^{-1}	MnO$_2$	2 M KNO$_3$	2	2.1	140	1 000	0.54	5
3	AC 2800 m^{2}g^{-1}	MnO$_2$	0.1 M K$_2$SO$_4$	2.2	n.d	124 (+150; -130)	5 000	n.d.	32
4	AC kuraray 1600 m^{2}g^{-1}	MnO$_2$	0.1 M Ca(NO$_3$)$_2$	2.0	3.17	124 (+314; -80)	1 000	9.0	33
5	AC PICACTIF 2300 m^{2}g^{-1}	MnO$_2$	0.1 M K$_2$SO$_4$	2	1.65	80 (+72; -95)	195 000	1.30	34
6	AC Ningde Xinseng Chem 2800 m^{2}g^{-1}	MnO$_2$	0.5 M K$_2$SO$_4$	2	1	153	10 000	3.20	35
7	AC	MnO$_2$	1 M LiOH	1.0	1	248	< 1500	n.d	36
8	AC Ningde Xinseng Chem 2800 m^{2}g^{-1}	MnO$_2$	0.5 M K$_2$SO$_4$	1.8	1	215	23 000	n.d.	37
9	AC 1300 m^{2}g^{-1}	MnO$_2$	1 M Li$_2$SO$_4$	2	1	212	n.d	~ 10-15	38

It is well known that redox phenomena associated with manganese oxide-based positive electrodes play an important role in the final capacitance of an ASC. Moreover, any variation in the pseudocapacitance of the positive electrode influences the capacitance behaviour of the carbon-based negative electrode [4-5, 28, 31]. Therefore, to explain the capacitance behaviour of these electrodes the influence of more parameters, such as the morphology and structure of the manganese oxide, whether it is amorphous or crystalline, the transport of cations (Na$^+$, H$^+$) to the pores and electron conduction of the bulk together with the redox reaction process must be taken into consideration [17, 32]. Water of MnO$_2$ structure is also thought to play an important role in ionic transport, while electronic conductivity is likely to be influenced by the bulk material properties of the electrode.

The results of the present work on carbon/MnO$_2$ supercapacitors are compared with those of the literature and presented in Table 4 [5, 32-38]. This table includes the composition of the electrodes, the types of electrolyte and the electrochemical characteristics of the ASC. From an analysis of the data, it is evident that the negative electrode is based on activated carbon materials and that the most

frequently used electrolyte was K_2SO_4 or other neutral salts with the exception of those reported by Yuan et al. [36]. They report of using 1M LiOH as electrolyte. Although they claim a high capacitance (~ 250 F g^{-1}) they had to use a cell voltage lower than 1 V because of the limited stability of manganese oxide in a basic aqueous medium [39-40]. Moreover, these authors observed a remarkable loss of capacitance (15-20%) during a cycling test of 1500 cycles. From an analysis of the literature it is evident that our work is the only one to report a good capacitance performance for carbon xerogel-based ASC, whereas the other works report results for supercapacitors based on activated carbon. In fact, the value of 213 F g^{-1} reported in this paper is relatively high compared to those reported by other authors. Another evident advantage of our ASC is its low resistivity, 0.28 Ω cm^2, which is considerably lower than those reported by Qu et al. [37] and Xue et al. [38] even though they reported similar high capacitances (i.e. 215 and 212 F g^{-1}). However, it is not clear from their report how it is possible to obtain these high values of capacitance using ASC of high resistance and with a negative and positive electrode weight ratio of 1:1. In our work we used a weight ratio of 2.65, which is similar (from 1.6 to 3.17) to those reported by other authors [5, 32-34]. Moreover, the manganese oxide-based positive electrode can be expected to provide a higher capacitance than the carbon-based negative electrode because of the high contribution of pseudocapacitance in a neutral aqueous electrolyte.

Analysis of the results of the literature (Table 4) also reveals discrepancies concerning the exact weight ratio between the negative and the positive electrodes. Moreover, the data of Table 4 do not allow evidencing a clear window of cell voltage used for this type of ASC because of the large differences. These points, however, are as important as the resistance of the electrolyte, the resistivity of the electrodes and the cycling stability of the ASC for improving capacitance performance. In short further studies are necessary to find out how the different characteristics of electrodes and electrolytes influence the electrochemical performance of supercapacitor devices. In this work, we have demonstrated that carbon xerogel (AOX6.5C) of a high BET surface area (~ 2300 m^2 g^{-1}) can be used to prepare negative electrodes (load ~ 8 mg cm^2) coupled with manganese oxide in positive electrodes (load of 3.6 mg cm^2) to design an ASC with a low resistivity, high specific capacitance and energy density of 15.1 W kg^{-1}. This latter is calculated considering the sum of the weight of active material in both electrodes.

Although no conclusive findings were made with respect to the importance of the faradaic and capacitive contributions, a high capacitance value of 213 F g^{-1} was achieved using an ASC with carbon xerogel and manganese oxide. This result indicates that these materials are very attractive for new potential applications in mild aqueous electrolyte-based asymmetric supercapacitors.

4. CONCLUSIONS

Different self-supporting electrodes based on carbon xerogels were prepared and their performance was studied in symmetric supercapacitors in an aqueous electrolyte (0.1 M Na_2SO_4).

The study revealed the important role that meso and macropores play in electrode resistance. It was also found that even when the samples had similar surface areas the capacitances of their supercapacitors differed considerably (from 30 to 70 F g^{-1}).

When a carbon xerogel was chemically activated with H_3PO_4 the surface area increased up to 2360 m^2 g^{-1}. An asymmetric supercapacitor with chemically activated carbon xerogel as negative electrode and manganese oxide as positive electrode made it possible to increase the working voltage from 1 to 1.6 V. The main advantages of using an asymmetric rather than a symmetric supercapacitor are that it provides a higher specific capacitance (213 F g^{-1} vs 90 F g^{-1}); and a higher specific energy (15.1 vs 3.2 Wh kg^{-1}).

The capacitance performance of an ASC can be further improved by increasing the capacitance of the carbon material-based negative electrode because of excellent behaviour of MnO_2-based positive electrode, which may achieve a capacitance as high as 300 F g^{-1}. Comparison of the results of this study with those of the literature showed that additional optimizations and improvements are necessary before MnO_2/carbon aqueous ASCs can be considered as a serious alternative to carbon/carbon non-aqueous commercial SSCs. Future optimization will need to consider the materials and the weight ratio for the electrodes as well as the resistivity, window cell voltage and cycling stability of the supercapacitors.

References

1. R. Kotz, M. Carlen, *Electrochimica Acta*, 45 (2000) 2483
2. P. Simon, Y. Gogotsi, *Nature Mater.*, 7 (2008) 845
3. E. Frackowiak, F. Beguin, *Carbon*, 39 (2001) 937
4. M. Toupin, T. Brousse, D. Belanger, *Chem. Mater.,* 16 (2004) 3184
5. V. Khomenko, E. Raymundo-Pinero, F. Beguin, *J. Power Sources,* 153 (2006) 183
6. K.Y. Kang, S.J. Hong, B.I. Lee, J.S. Lee, *Electrochem. Commun.*, 10 (2008) 1105
7. L. Zubizarreta, A. Arenillas, J.P. Pirard, J.J. Pis, N. Job, *Micropor. Mesopor. Mater.,* 115 (2008) 480
8. F.L. Conceicao, P.J.M. Carrott, M.M.L. Ribeiro Carrott, *Carbon,* 47 (2009) 1874
9. S.T. Mayer, R.W. Pekala, J.L. Kaschmitter, *J. Electrochem. Soc.,* 140 (1993) 446
10. H. Probstle, C. Schmitt, J. Fricke, *J. Power Sources,* 105 (2002) 189
11. J. Wang, X. Yang, D. Wu, R. Fu, M.S. Dresselhaus, G. Dresselhaus, *J. Power Sources,* 185 (2008) 589
12. E.G. Calvo, C.O. Ania, L. Zubizarreta, J.A. Menendez, A. Arenillas, *Energy Fuels*, 24 (2010) 3334
13. J. Jagiello, M. Thommes, *Carbon,* 42 (2004) 1227.
14. M.M. Dubinin In: J.F. Danielli, M.D. Rosenberg, D. Cadenhead (Eds.), *Progress in Surface and Membrane Science*, vol. 9, Academic Press, New York (1975), pp. 1–70.

15. F. Stoeckli, T.A. Centeno, *Carbon,* 43 (2005) 1184
16. T.A. Centeno, F. Stoeckli, *Electrochimica Acta,* 52 (2006) 560
17. P. Staiti, F. Lufrano, *J. Power Sources,* 187 (2009) 284
18. C. Moreno-Castilla, F.J. Maldonado-Hodar, *Carbon,* 43 (2005) 455
19. F. Lufrano, P. Staiti, *Int. J. Electrochem. Sci,* 50 (2010) 903
20. C.A. Thorogood, G.G. Wildgoose, A. Crossley, R. M. J. Jacobs, J.H. Jones, R.G. Compton, *Chem. Mater.,* 19 (2007) 4964
21. H. A. Andreas, B. E. Conway, *Electrochimica Acta,* 51 (2006) 6510
22. Q. T. Qu, B. Wang, L. C. Yang, Y. Shi, S. Tian, Y. P. Wu, *Electrochem. Commun.,* 10 (2008) 1652
23. L. Zhang; H. Liu, M. Wang, L. Chen, *Carbon,* 45 (2007) 1439
24. F. Lufrano, P. Staiti, M. Minutoli, *J. Electrochem. Soc.,* 151 (2004) A64
25. H.K. Song, J.H. Sung, Y.H. Jung, K.H. Lee, L.H. Dao, M.H. Kim, H.N. Kim, *J. Electrochem. Soc.,* 151 (2004) E102
26. H.K. Song, J.H. Jang, J.J. Kim, S.M. Oh, *Electrochem. Commun.,* 8 (2006) 1191
27. S. Devaraj, N. Munichandraiah, *J. Electrochem. Soc.,* 154 (2007) A80
28. V. Khomenko, E. Raymundo-Pinero, E. Frackowiak, F. Beguin, *Appl. Phys. A-Mater.,* 82 (2006) 567
29. S.H. Kim, Y.I. Kim, J.H. Park, J.M. Ko, *Int. J. Electrochem. Sci*., 4 (2009) 1489
30. Q. L. Fang, D.A. Evans, S.L. Roberson, J.P. Zheng, *J. Electrochem. Soc.,* 148 (2001) A833
31. D. Belanger, T. Brousse, J.W. Long, *Electrochem. Soc. Interface,* 17 (2008) 49
32. T. Cottineau, M. Toupin, T. Delahaye, T. Brousse, D. Belanger, *Appl. Phys. A-Mater.,* 82 (2006) 599
33. C. Xu, H. Du, B. Li, F. Kang, Y. Zeng, *J. Electrochem. Soc.,* 156 (2009) A435
34. T. Brousse, P. L. Taberna, O. Crosnier, R. Dugas, P. Guillemet, Y. Scudeller, Y. Zhou, F. Favier, D. Belanger, P. Simon, *J. Power Sources,* 173 (2007) 633
35. Q. Qu, L. Li, S. Tian, W. Guo, Y. Wu, R. Holze, *J. Power Sources,* 195 (2010) 2789
36. A.Yuan, Q. Zhang, *Electrochem. Commun.,* 8 (2006) 1173
37. Q. Qu, P. Zhang, B. Wang, Y. Chen, S. Tian, Y. Wu, R. Holze, *J. Phys. Chem. C,* 113 (2009) 14020
38. Y. Xue, Y. Chen, M.-L. Zhang, Y.-D. Yan, *Mater. Lett.,* 62 (2008) 3884
39. M. Toupin, T. Brousse, D. Belanger, *Chem. Mater.,* 14 (2002) 3946
40. Q. Zhou, X. Li, Y.-G. Li, B.-Z. Tian, D.-Y. Zhao, Z.-Y. Jiang, *Chinese J. Chem.,* 24 (2006) 835